Novel Photovoltaic-Thermoelectric Temperature Control Using A Closed-Loop Integrated Cooler (CLIC)

Matthew H. Rolley[1*], Tracy K.N. Sweet[1], Gao Min[1]

[1]School of Engineering, Cardiff University, Cardiff. CF24 3AA

*RolleyMH@Cardiff.ac.uk

Abstract: The Closed-Loop Integrated Cooler (CLIC) is a novel technique deployed on experimental apparatus to accurately measure, monitor and control the temperature of optoelectronic devices. Demonstrated here within a Concentrator Photovoltaic-Thermoelectric (CPV-TE) hybrid device, the thermoelectric module was used as a solid state sensor and heat pump in order to control the operational temperature for a triple-junction solar cell. The technique was used to achieve stable, reproducible and repeatable Standard Test Conditions (STC) of 25°C cell temperature, with 1000W/m² irradiance and AM1.5G spectrum. During testing with Secondary Optical Element (SOE) optics in a solar simulator, the CLIC enabled accurate temperature control of the CPV cell. This would otherwise be unfeasible due to the spectral, reflective and diffusive effects of the SOE optics. The CLIC was used to obtain temporal and spatial constant temperature of the CPV-TE hybrid receiver during Current-Voltage measurement. This method highlights the future potential of the CLIC for accurate temperature control of optoelectronic devices both during testing and in future semiconductor device applications where temperature control is essential to performance or lifetime.

1. Introduction

Epitaxially grown III:V semiconductors have a plethora of uses in optoelectronics. One such application is as high-efficiency photovoltaic cells that can utilise complex multi-junction cell architectures to achieve world record photon conversion efficiency (PCE) into electricity. Multi-junction solar cell architectures, through their design, have different component sub-cell material bandgap voltages. This enables high efficiency conversion of the solar spectrum wavelengths (285nm-3000nm) incident upon the cell. State-of-the-art cells of this nature currently utilize four-junction designs with recent research challenges to provide the photovoltaic industry with a cell architecture that can have a sub-cell bandgap at 1.0eV, thereby increasing cell conversion efficiency towards 50%. The current world-record for this technology highlights a fabrication method of forming two dual-junction epitaxially grown sub cells grown on two different substrates, which are then wafer bonded producing the four-junction solar cell. Record cell efficiencies of 46% [1] have been reported with current research trends in both the space and terrestrial photovoltaic industries to increase the number of material bandgaps/junctions [2] to capitalise on further sub cell bandgap optimisation. Current state-of-the-art solar cell for higher volume manufacture are triple-junction cells with a slightly lower conversion efficiency. The trade-off of a simpler manufacture process and lower cost per wafer/cell. These solar cells have lattice-matched sub cell compositions of GaInP top cell (UV-VIS wavelengths), a GaInAs middle sub cell (VIS wavelengths) grown onto a bottom Ge substrate (VIS-IR wavelengths) and achieve representative conversion efficiencies over 40% [3]. The high conversion efficiency of these cells used in combination with low cost concentrating optics can offset the comparatively high market cost compared to lower efficiency first or second generation silicon-based technologies.

High optical concentration can be achieved through the use of "Primary Optical Elements" (POEs) of low-cost Fresnel Lenses, or alternative high-cost achromatic doublet lenses. "Secondary Optical Elements" (SOEs) are typically also included in the optical path, to homogenise the incident light flux in spatial or spectral distribution, potentially correcting for POE detrimental Chromatic Aberration (CA) effects. This increases the effective concentration ratio (CR). Typical CRs of deployed Concentrator Photovoltaic (CPV) systems are in the region of 500x, with the trend being to push for higher CRs [4]. High CPV (HCPV) systems have been proposed with CRs of up to 1000x to be economically feasible [5]. Far from being impractical, CPV has achieved competitive $/W energy generation costs in countries with a DNI (Direct Normal Irradiance) of greater than 1500Wm^{-2} [6]. Multi-junction solar cells have a smaller temperature co-efficients compared to Silicon through minimising parasitic thermalisation losses within the cell [7]. As the designed concentration ratios are increased, improving CPV profit returns through a better system design Levelized Cost of Energy (LCOE), cell temperature monitoring and metrology becomes critical to cell lifetime performance.

Thermoelectrics are solid-state semiconductor devices which can generate temperature differentials from an applied current or likewise convert temperature gradients (δT) directly to electrical power. These two mechanisms are called the Peltier and Seebeck effects respectively [8]. For room temperature applications ($\delta T < 100^{o}C$), the majority of modules use Bismuth Telluride active material (Bi_2Te_3) with typical co-efficients of performance of approximately 1 [9]. Thermoelectrics have been a well-established technique for solid state cooling in niche applications such as the cooling of advanced photonic devices and lasers [10, 11]. Recent technology directions for CPV devices specifically has included the research of hybrid receivers which seamlessly integrate these two semiconductor technologies into one optimised CPV-TE device. Preliminary work has investigated

these devices with photovoltaic technologies such as GaAs cells [12], organic based solar cells [13, 14] and monocrystalline silicon cells [15]. Likewise, theoretical and numerical simulations exist for multi-junction CPV-TE hybrids [16, 17], but experimental realisations of these devices are scarce [18-20].

2. CLIC Device Overview and Experimental Calibration

Current experimental metrology for the temperature evaluation of solar cells include k-type and PT100 type thermocouples, Forward Looking Infrared (FLiR) thermal imaging cameras, and Infrared (IR) thermometers. However, these techniques all have inherent drawbacks – especially with hybrid architectures. Any front contacted temperature measurements create cell shading effects and rear-contact measurements are inaccurate. By definition, optoelectronics need their active area to be free of obstruction to eliminate any shading or subtractive blocking effects for their output or generation. Spatial location of a thermocouple is paramount for measurement accuracy, and as described by Fourier's law of conduction a δT will be exhibited with non-zero distances. Due to the supporting circuitry and contacts needed for optoelectronic devices, the unavoidable separation distance between the thermocouple attachment and desired measurement area will generally be larger than with rear mounting. IR thermometer based contactless measurements avoid the complications of mechanical attachment and thermocouple spatial inaccuracy, but come with different limitations. Here instead, the specified IR device measurement accuracy is only applicable when used at the device calibrated focal plane. Measurements are assumed to be taken with the sample perpendicular to the IR sensor, something infeasible whilst avoiding cell/device shading. FLiR cameras are excellent at recording thermal distribution information but the thermal emissivity selected, defined in the measurement procedure, is critical to measurement accuracy [21]. Furthermore, similar to IR thermometers, use of the device at non-perpendicular angles can also exhibit spectral diffusion and reflection effects in the received reading and hence give spurious/inaccurate output data. Additionally the emitted IR radiation from the sensor itself can be converted by the bottom Germanium junction with the solar cell, and as such can create a spurious or skewed cell conversion output. As described above, a thermoelectric module (TEM) can generate a proportional voltage through the Seebeck effect from a temperature difference. The magnitude of the temperature differential, the TEM hot side temperature and hence the absolute cell temperature can be back-calculated. This was done using the module Seebeck co-efficient (α) and a cold side reference measurement. The TEM can then be driven in Peltier mode by supplying a current and establishing a contrary temperature differential. Acting as a heat pump, effective solid-state cooling was achieved with a high sensitivity by combining these two processes. Additionally, by using these two phenomena within a Proportional-Integral-Derivative (PID) control algorithm framework, accurate and steady-state device temperatures were achieved. In previous work [22], the Seebeck co-efficient (α) for the TEM was measured experimentally using a bespoke testing rig. A range of δTs was applied to the TEM and open circuit voltages (V_{oc}) of the module recorded. The test rig was first evaluated using a COMSOL model, Figure 1, to investigate any thermal distribution in-homogeneities and hence parasitic inaccuracies from TEM thermal resistances upon the calibration rig. Fixed temperature boundary conditions of a hot side temperature of 30°C and a cold side temperature of 10°C were used to investigate the TEM's influence on temperature distribution.

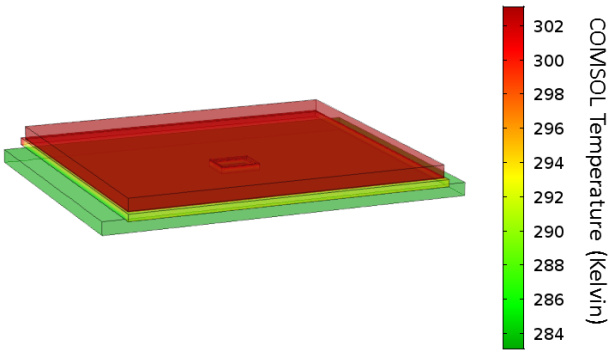

Figure 1. *COMSOL study showing uniform simulated temperature distributions for CLIC calibration rig. Note that no TEM-induced hotspots were shown, hence temperature distribution homogeneity was maintained.*

It was shown that the copper within the calibration rig had a sufficient thermal mass to eliminate these detrimental effects and maintain temperature calibration accuracy. Figure 2 shows an overview of the experimental setup used in combination with the calibration rig for evaluation of the thermoelectric parameters. The experimental setup consisted of a resistive heater (200Ω nominal resistance at 25°C) powered by a variable laboratory power supply (rated max 60V, 0.5A, 30W output) giving hot-side temperatures up to 80°C, and hence δTs up to 70°C. The CLIC experimental rig included location holes for two k-type thermocouples which were used with a FLUKE 52 Series II thermometer as the temperature measurement calibration datum. The V_{oc} data obtained for the thermoelectric was fitted to a linear trend line as can be approximated from the established material figure of merit for this δT range, and calibration co-efficients were extracted. These co-efficients were applied in proof-of-concept Arduino source code, and temperatures were back-validated by using the CLIC temperature measurement itself

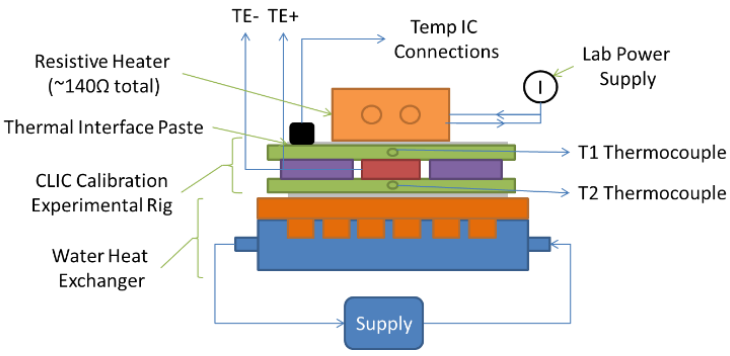

Figure 2. *CLIC calibration experimental setup.*

in the test rig to "predict" the temperature on a prototype circuit. This process evaluated a preliminary CLIC measurement technique accuracy as compared to the thermocouples within the rig with max error of +0.99ºC to -1.08ºC. The CLIC measurements as compared to the thermocouple datum are shown in Figure 3.

3. The Hybrid CPV-TE Receiver and Experimental Deployment of the CLIC

The CLIC was used to control the CPV cell temperature as part of a larger experimental setup with the CPV-TE hybrid receiver. The electrical performance I-Vs were measured at STC conditions (25ºC, 1000Wm^{-2} at AM 1.5G). The cell temperature readings from the CLIC were used as an additional recorded receiver variable, whilst also serving as a practical deployment demonstration and evaluation of the technique efficacy. A labelled photograph of the characterised hybrid receiver is given in Figure 4. The hybrid receiver was tested under a Lot Oriel ABB class solar simulator and at an irradiance plane of 1000Wm^{-2} calibrated using a Kipp and Zohan CMP11 pyranometer with sensitivity 9.01µV/Wm^{-2}. For higher accuracy experimental realisation of the CLIC temperature measurement technique, a Keysight 34972A data-logger installed with a 34901A 20-channel multiplexor was used here to monitor the Seebeck generated V_{oc} of the TEM within the hybrid device. This data logger also recorded the ambient temperature (TAmbient) using a J-type thermocouple, and the receiver base temperature (TCold) with a k-type thermocouple as the cold-side reference datum for the CLIC measurement. The experimental setup used is shown in Figure 5.

An algorithm was written for use with the Keysight Data logger 3 software to apply the Seebeck co-efficients as found in the CLIC calibration experiment above, to the TEM measurement and hence record the calculated δT for the CLIC alongside other receiver metrology data. The cold-side thermocouple was placed within the hybrid receiver inside a hole drilled to the geometrical centre of the substrate and used with thermally conductive paste to ensure a good thermal contact. I-V and P-V curves for the solar cell in the CPV-TE hybrid receiver were then taken using an AUTOLAB potentiostat system, at four different temperatures (23ºC, 25ºC, 56ºC, and 71ºC) controlled and measured with the

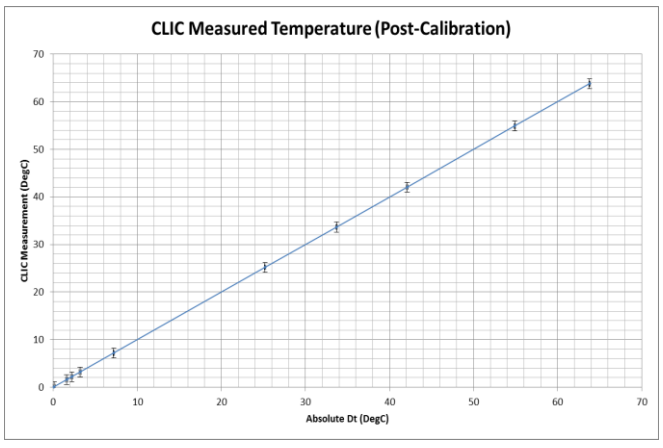

Figure 3. *Measurement Calibration Data for CLIC*

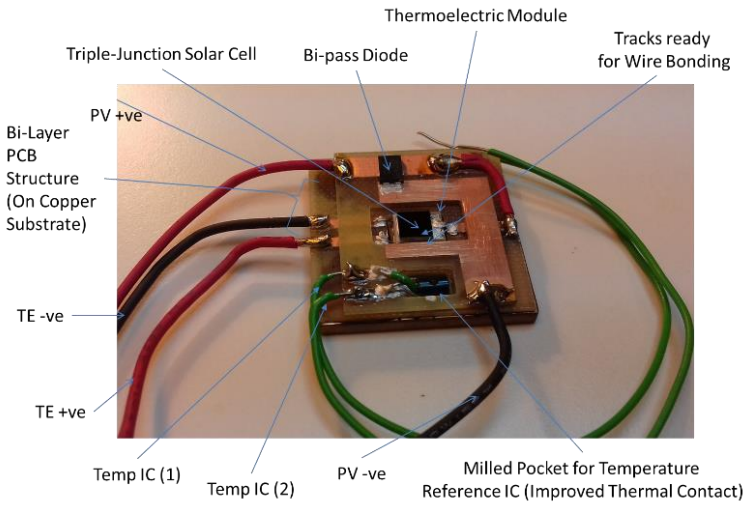

Figure 4. *CPV-TE receiver photograph.*

CLIC. All temperatures and measurements were recorded every second, with an I-V scan taking a total of 30 seconds (30 readings) to complete. This time resolution was chosen to log the data accurately whilst minimising output file size.

The temperature controlled and recorded by the CLIC show exceptional linearity over the range of each I-V scan, regardless of absolute temperature. These consistent temperatures show the efficacy and accuracy of the CLIC technique and apparatus for use in temperature-sensitive optoelectronic device testing. Close agreement under steady-state operation for the solar cell was achieved when comparing cell I-V parameters the short-circuit current I_{sc} and V_{oc} with previous STC testing data of the cell, with minimal temperature shift in the data likewise being exhibited in the curve. CLIC temperature measurement were applicable in this deployment application, regardless of detecting a negative or positive temperature difference between the cell temperature and the cold side temperature of the receiver substrate or water heat exchanger temperature. The time-

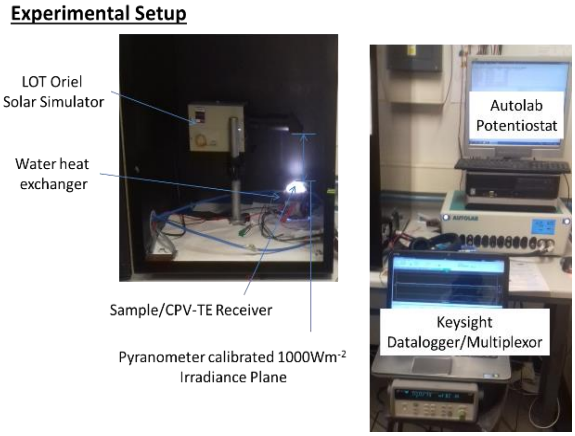

Figure 5. *Experimental setup used for CLIC deployment and CPV-TE hybrid receiver evaluation*

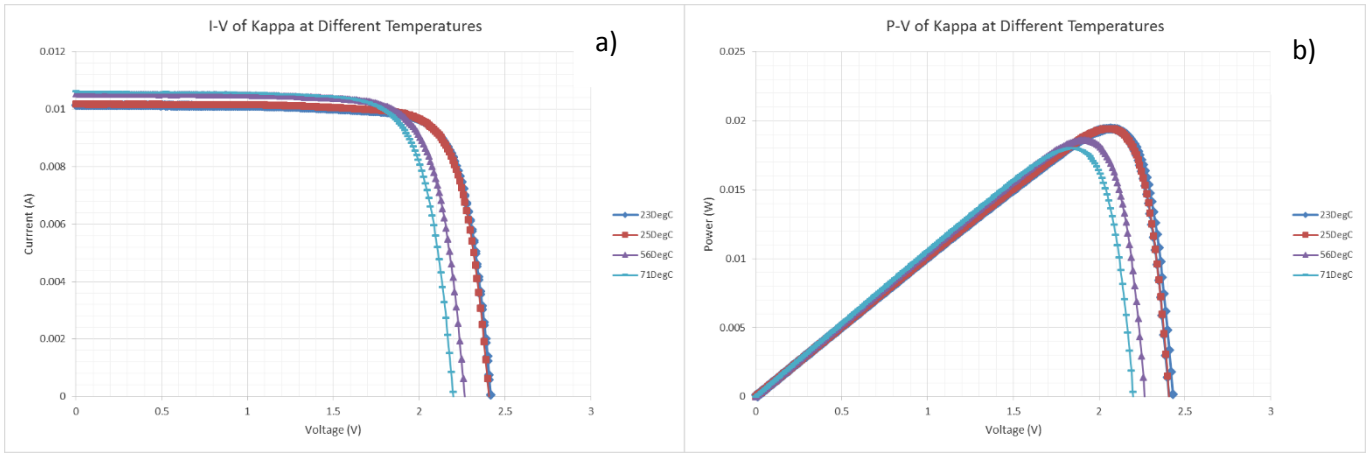

Figure 6. (a) *Current-Voltage curves, and* ***(b)*** *Power-Voltage Curves obtained from the CPV-TE hybrid receiver under CLIC-controlled steady state temperature conditions*

resolved data obtained from the data logger is summarised in Figure 7 (a) to (d).

4. Results

For electrical evaluation, the current-voltage (I-V) scans of the CPV-TE receiver were measured and are plotted in Figure 6 (a). As has been well established in literature [23, 24] the I_{sc} increased and the V_{oc} decreased with increasing temperature. This is due to the bandgap shift induced from this applied temperature change, with the increase in current generation reflecting a drop in the junction potential barrier [25, 26]. Hence a larger amount of lower energy charge carriers flow through the junction. This temperature rise resulted in an overall net drop in conversion efficiency and hence reduction in absolute power generation – as was also shown by the comparative power-voltage (P-V) curves, plotted in Figure 6 (b). Due to the small thermal mass of the solar cell and the inherent fast thermal time constant of the solid-state TEM, high measurement sensitivity was achieved. From this high resolution a number of temperature artefacts were recorded throughout the I-V scan procedure when active CLIC temperature compensation was switched off. This included temperature spikes of approximately 1ºC for all tests when the cell was driven into the forward bias (FB) condition

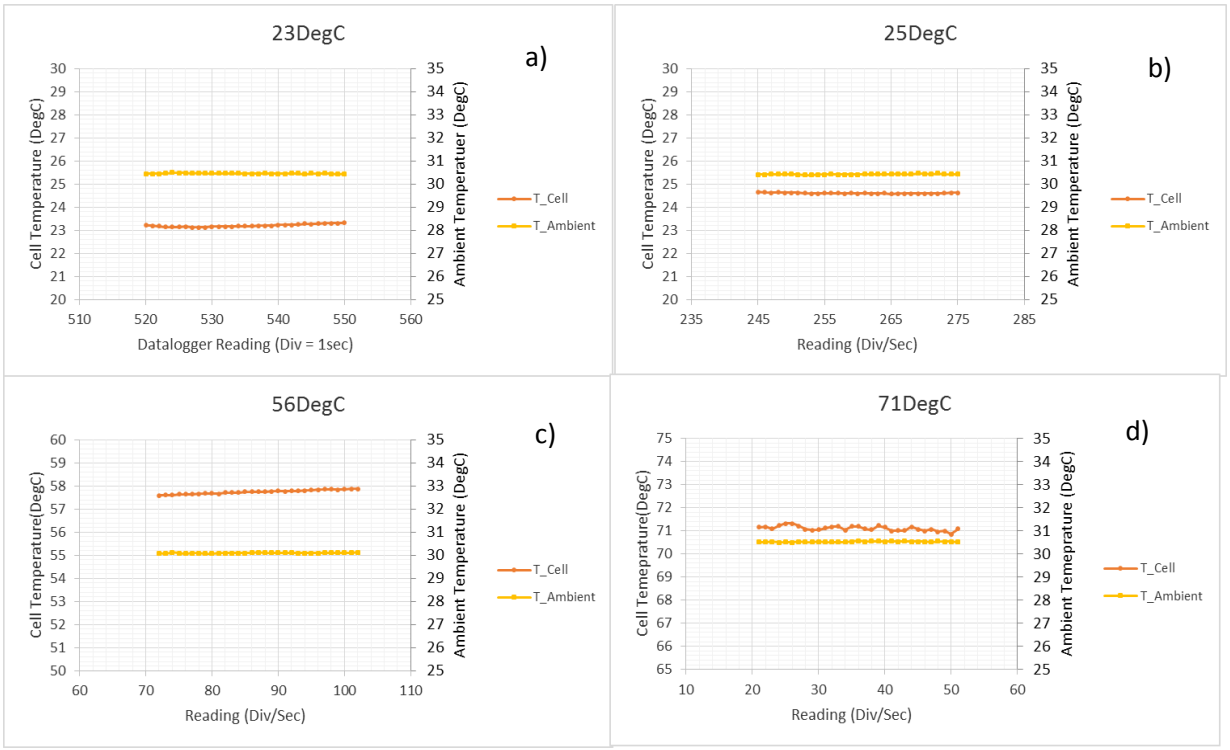

Figure 7. *Time-resolved temperature recordings from the experimental data logger setup, for each temperature (CLIC-Compensated) applied to the CPV-TE receiver:* ***(a)*** *23ºC,* ***(b)*** *25ºC,* ***(c)*** *56ºC,* ***(d)*** *71ºC.*

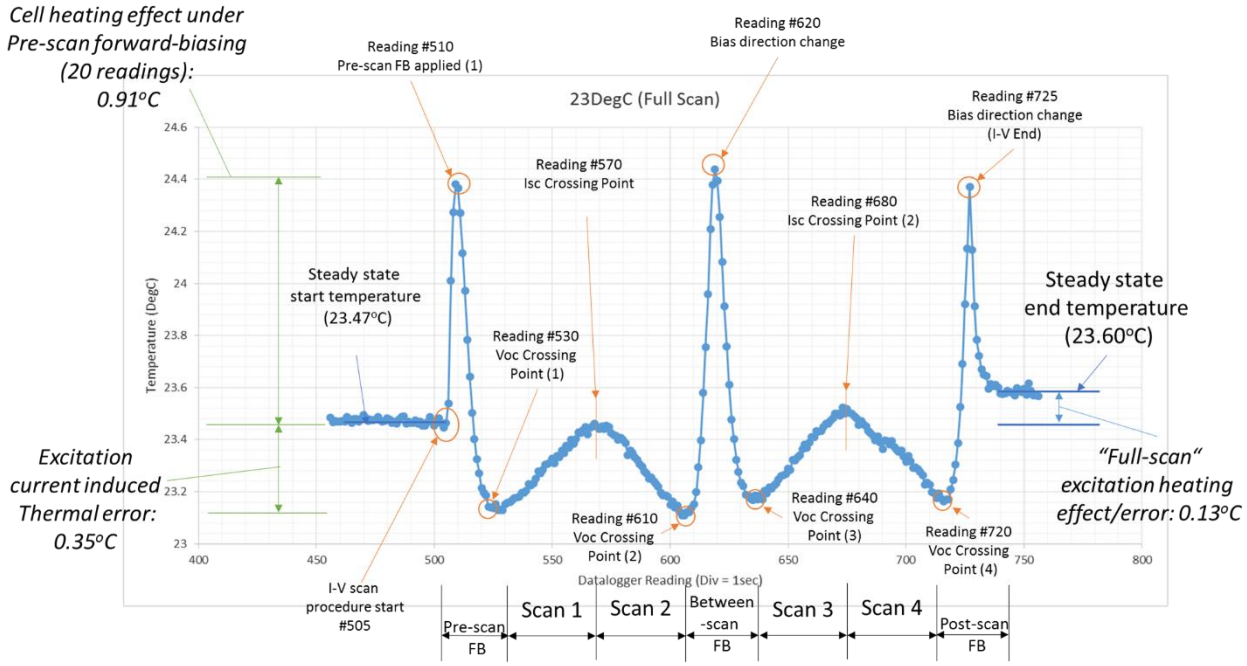

Figure 8. *Full CLIC measured temperature trace obtained through an I-V scan taken at 23°C.*

from the AUTOLAB procedure. Using temperature co-efficient data on these solar cells previously published by the authors, this spike could equate to an I-V measurement Voc error of -4.5512×10^{-3} V, and a $+1.1596 \times 10^{-5}$ A I_{sc} error. This heating effect can be expected from the FB excitation condition to the cell internal shunt resistance. Additionally, increasing temperature gradients were shown when the biasing current tended toward its maximum condition, the I_{sc}. Demonstrated on the I-V scan conducted at 23°C (see Figure 7, a), this high sensitivity temperature data and observed artefacts summarised displayed in Figure 8. An overall excitation current induced thermal error was measured as compared to the pre-scan steady-state temperature achieved of 0.3°C. The full I-V scan procedure caused a 0.13°C overall cell temperature increase. With more temperature-critical devices under test, these measurement procedure-induced temperature artefacts have the potential to induce measurement and hence characterisation inaccuracies.

5. Conclusions

A novel temperature metrology technique to counteract the limitations of existing infrared and thermocouple based techniques was developed. The CLIC measurement technique was calibrated using a bespoke experimental calibration rig, with preliminary simulations evaluated in COMSOL and using thermocouples as its datum. The technique was then deployed in conjunction with a data logger, to evaluate the electrical characteristics of a CPV-TE hybrid receiver with a SOE. The electrical I-V and P-V curves of the CPV cell were obtained at various CLIC-controlled steady-state temperatures, with the cell temperature being simultaneously measured and controlled using the same thermoelectric device. Additionally, the high temperature sensitivity of the CLIC technique enabled the observation of sub-degree I-V scan temperature data and deviation artefacts. These were recorded and analysed alongside the steady state thermal logging data. Throughout CLIC active compensated I-V scans on the receiver, minimal temporal deviation of the I-V traces was shown. The potential of the CLIC was demonstrated for both effective experimental metrology and for real-world deployment to control and measure the temperature of an optoelectronic device using a thermoelectric module. Future work will include developing a simplified circuit for ease-of-manufacture, and using the CLIC as a tool to further investigate CPV-TE hybrid receivers.

6. Acknowledgements

The authors would like to thank the Sêr Cymru National Research Network (http://www.ernw.ac.uk/en/) for financial support, IQE plc for supply of III:V triple-junction cells, Cardiff School of Physics for cleanroom facilities, and EPSRC SUNTRAP consortium (EP/K022156/1) for collaboration.

7. References:

1. Dimroth, F., T.N.D. Tibbits, M. Niemeyer, et al., *Four-Junction Wafer-Bonded Concentrator Solar Cells.* IEEE Journal of Photovoltaics, 2016. **6**(1): p. 343-349.
2. King, R.R., D. Bhusari, D. Larrabee, et al., *Solar cell generations over 40% efficiency.* Progress in Photovoltaics: Research and Applications, 2012. **20**(6): p. 801-815.
3. King, R.R., D.C. Law, K.M. Edmondson, et al., *40% efficient metamorphic GaInP/GaInAs/Ge multijunction solar cells.* Applied Physics Letters, 2007. **90**(18): p. 183516.

4. Shanks, K., S. Senthilarasu, and T.K. Mallick, *Optics for concentrating photovoltaics: Trends, limits and opportunities for materials and design.* Renewable and Sustainable Energy Reviews, 2016. **60**: p. 394-407.
5. Talavera, D.L., P. Pérez-Higueras, F. Almonacid, et al., *A worldwide assessment of economic feasibility of HCPV power plants: Profitability and competitiveness.* Energy, 2017. **119**: p. 408-424.
6. Fairley, P., *New Scientist Gamechangers: Energy*. 2015, New Scientist.
7. Fernández, E.F., G. Siefer, M. Schachtner, et al., *Temperature coefficients of monolithic III-V triple-junction solar cells under different spectra and irradiance levels.* AIP Conference Proceedings, 2012. **1477**(1): p. 189-193.
8. Rowe, D.M., *CRC handbook of thermoelectrics*. 1995: CRC press.
9. Goldsmid, H.J., A.R. Sheard, and D.A. Wright, *The performance of bismuth telluride thermojunctions.* British Journal of Applied Physics, 1958. **9**(9): p. 365.
10. Bell, L.E., *Cooling, heating, generating power, and recovering waste heat with thermoelectric systems.* Science, 2008. **321**(5895): p. 1457-1461.
11. Enright, R., S. Lei, G. Cunningham, et al., *Integrated Thermoelectric Cooling for Silicon Photonics.* ECS Journal of Solid State Science and Technology, 2017. **6**(3): p. N3103-N3112.
12. Xu, X., S. Zhou, M.M. Meyers, et al., *Performance analysis of a combination system of concentrating photovoltaic/thermal collector and thermoelectric generators.* Journal of Electronic Packaging, 2014. **136**(4): p. 041004.
13. Zhou, Z., J. Yang, Q. Jiang, et al., *Large improvement of device performance by a synergistic effect of photovoltaics and thermoelectrics.* Nano Energy, 2016. **22**: p. 120-128.
14. Zhang, J., Y. Xuan, and L. Yang, *A novel choice for the photovoltaic–thermoelectric hybrid system: the perovskite solar cell.* International Journal of Energy Research, 2016.
15. Fisac, M., F.X. Villasevil, and A.M. López, *High-efficiency photovoltaic technology including thermoelectric generation.* Journal of Power Sources, 2014. **252**: p. 264-269.
16. Rezania, A., D. Sera, and L. Rosendahl, *Coupled thermal model of photovoltaic-thermoelectric hybrid panel for sample cities in Europe.* Renewable Energy, 2016. **99**: p. 127-135.
17. Cui, T., Y. Xuan, and Q. Li, *Design of a novel concentrating photovoltaic–thermoelectric system incorporated with phase change materials.* Energy Conversion and Management, 2016. **112**: p. 49-60.
18. Beeri, O., O. Rotem, E. Hazan, et al., *Hybrid photovoltaic-thermoelectric system for concentrated solar energy conversion: Experimental realization and modeling.* Journal of Applied Physics, 2015. **118**(11): p. 115104.
19. Sweet, T.K., M. Rolley, G. Min, et al. *Scalable solar thermoelectrics and photovoltaics (SUNTRAP)*. in *AIP Conference Proceedings*. 2016. AIP Publishing.
20. Sweet, T.K.N., M.H. Rolley, M.J. Prest, et al., *Novel hybrid III:V concentrator photovoltaic-thermoelectric receiver designs.* AIP Conference Proceedings, 2017. **1881**(1): p. 080009.
21. Rogalski, A. and K. Chrzanowski, *Infrared devices and techniques.* 2002.
22. Rolley, M.H., T.K.N. Sweet, and G. Min, *In-situ thermoelectric temperature monitoring and "Closed-loop integrated control" system for concentrator photovoltaic-thermoelectric hybrid receivers.* AIP Conference Proceedings, 2017. **1881**(1): p. 100001.
23. Kinsey, G.S., P. Hebert, K.E. Barbour, et al., *Concentrator multijunction solar cell characteristics under variable intensity and temperature.* Progress in Photovoltaics: Research and Applications, 2008. **16**(6): p. 503-508.
24. Siefer, G. and A.W. Bett, *Analysis of temperature coefficients for III–V multi-junction concentrator cells.* Progress in Photovoltaics: Research and Applications, 2014. **22**(5): p. 515-524.
25. Dupré, O., R. Vaillon, and M.A. Green, *Physics of the temperature coefficients of solar cells.* Solar Energy Materials and Solar Cells, 2015. **140**: p. 92-100.
26. Singh, P. and N.M. Ravindra, *Temperature dependence of solar cell performance—an analysis.* Solar Energy Materials and Solar Cells, 2012. **101**: p. 36-45.